Title: Generation of neuronal diversity from common progenitors via Notch signaling in the cerebellum

Short title: Notch regulates cerebellar neuronal diversity

Tingting Zhang[1,2], Tengyuan Liu[1,2], Natalia Mora[1], Justine Guegan[1], Mathilde Bertrand[1], Ximena Contreras[3], Andi H. Hansen[3], Carmen Streicher[3], Marica Anderle[4], Luca Tiberi[4], Simon Hippenmeyer[3] and Bassem A. Hassan[1]

1: Institut du Cerveau (ICM), Sorbonne Université, Inserm, CNRS, Hôpital Pitié-Salpêtrière, Paris, France.

2: Doctoral School of Biomedical Sciences, KU Leuven, 3000 Leuven, Belgium

3: Institute of Science and Technology Austria, Am Campus 1, 3400 Klosterneuburg, Austria

4: Armenise-Harvard Laboratory of Brain Disorders and Cancer, CIBIO, University of Trento, Via Sommarive 9, 38123 Trento, Italy

Summary

The bewildering diversity of brain neurons arises from relatively few pluripotent progenitors through poorly understood mechanisms. The cerebellum is an attractive model to investigate mechanisms of neuronal diversification because the different subtypes of excitatory and inhibitory neurons are well described [1,2]. The cerebellum is a hub for control of motor function and contributes to a number of higher brain functions such as reward-related cognitive processes [3]. Deficits in cerebellar development lead to severe neurological disorders such as cerebellar ataxias [4] and medulloblastomas [5], a heterogeneous and severe groups of childhood brain tumors, thus underlying the importance of understanding the cellular and molecular control of cerebellar development. In contrast to text book models, we report that excitatory and inhibitory cerebellar neurons derive from the same pluripotent embryonic cerebellar stem cells (eCSC). We find that the excitatory versus inhibitory fate decision of a progenitor is regulated by Notch signaling, whereby the cell with lower Notch activity adopts the excitatory fate, while the cell with higher Notch activity adopts the inhibitory fate. Thus, Notch-mediated binary cell fate choice is a conserved strategy for generating neuronal diversity from common progenitors that is deployed at different developmental time points in a context specific manner.

Body text

Cerebellar anlagen

Text book models suggest that different cerebellar neurons arise from two distinct progenitor pools (Fig.S1A) located either dorsally in the rhombic lip (RL) or ventrally in the ventricular zone (VZ). Two basic helix-loop-helix (bHLH) transcription factors called Atonal homologue 1 (Atoh1; RL) and Pancreas transcription factor 1 alpha (Ptf1a; VZ), mark these progenitors. Atoh1^{+} RL progenitors give rise to glutamatergic neurons, while Ptf1a^{+} VZ progenitors give rise to GABAergic neurons [6]. However, pseudo-time trajectory analysis of single-cell RNAseq (scRNAseq) embryonic mouse cerebellum data suggests that a common pool of progenitors branches into either a glutamatergic fate or a GABAergic fate [7]. In addition, cell fate in the two germinal niches can be switched when Atoh1 and Ptf1a are ectopically expressed in the VZ and RL, respectively [8,9]. Finally, the classic neural stem cell marker Sox2 is an early VZ marker, but cells expressing both Sox2 and the RL marker Atoh1 were observed in human cerebellar organoids [10]. Whether this means that common pluripotent progenitors competent to generate both excitatory and inhibitory lineages exist, and how this binary fate decision is regulated, are unknown.

Characterization and fate mapping of embryonic Cerebellar Stem Cells

We observed Sox2 protein expression in VZ and RL during cerebellar neurogenesis (E9.5 – E16; Fig.1SB-F). Furthermore, some Sox2^{+} cells express Atoh1 (Fig.1SB'-F'). This suggests that Sox2^{+} progenitors may represent a pool of eCSCs generating both excitatory and inhibitory lineages. To test this, we performed lineage tracing in *Sox2*^{CreERT2}*/Gt(ROSA)26Sor*^{tdTomato}*/Atoh1*^{GFP} mice using low doses of Tamoxifen (TM: 0.1mg, 0.03mg). Under both conditions, in all mice examined, Sox2^{+} cells and their progeny labelled with tdTomato (tdTomato+). We observed Ptf1a^{+}/tdTomato^{+} and Atoh1^{+}/tdTomato^{+} cells at E12.5 in the VZ and RL, respectively (Fig. 1A-F''). At postnatal day 21 (P21) we found tdTomato^{+} Purkinje cells (PCs, Calbindin^{+}), granule cells (GCs, Pax6^{+}), glutamatergic deep cerebellar nuclei (glu-DCN, Olig2^{+}, Pax6^{+} and Tbr1^{+}) and GABAergic interneurons (INs, Pax2^{+}), suggesting they all come from Sox2^{+} eCSCs (Fig.1G-N and S2).

To characterize the progeny of single eCSCs, we employed the sparse clonal Mosaic Analysis with Double Markers (MADM) technology [11,12]. Briefly, depending on how the red and green markers segregate after recombination, the two hemi-lineages of a common progenitor would label either in red versus green or in yellow versus no-label (Fig. 2A). Thus, the presence of rare clones strictly containing either different cell types in the two different colors, or only one cell type in yellow, is consistent with recombination in a common progenitor. More importantly, failure to find such clones indicates lack of common progenitors. Consistent with sparsity of MADM clones [11,12], TAM injection at E11 generated an average of 0.42 MADM events per brain (13 in 31 brains). In 2 clusters, we observed GABAergic and glutamatergic cells in different colors, containing GCs, PCs and cerebellar INs (Fig. 2B-G and S3C-F) providing direct evidence for a common progenitor. In 6 clusters, we detected either GABAergic lineages (PCs or INs) or Glutamatergic lineage (GCs) in yellow (Fig. 2H-I and S3G-G''), but not both. In the remaining 5 clusters, sparse green or red GABAergic lineages were observed (Fig. S3A-B), indicating recombination occurred in fate-restricted precursors. Consistent with the fact that GC precursors undergo transient amplification before neurogenesis, while PC precursors do not, all MADM clones contained more GCs than PCs. We asked if pluripotent eCSC are present in human. We sparsely labelled Sox2$^+$ eCSCs by electroporating Sox2Cre/Venus vectors into human-iPS-derived cerebellar organoids and traced their fate after 16 days in culture. In each organoid, we observed both PCs (Venus$^+$/Calbindin$^+$) and GCs (Venus$^+$/Pax6$^+$) (Fig. 2J-O'''). Altogether, lineage tracing data show that Sox2$^+$ eCSCs give rise to two lineage-restricted precursors that generate both GCs and PCs.

Notch signaling regulates the fate of embryonic Cerebellar Stem Cells and their progeny

To identify the molecular underpinnings of the diversification of cerebellar neurons from common progenitors, we analyzed available scRNAseq data from E10-E13 mouse cerebella (ENA: PRJEB23051 [13]) to define the molecular features of eCSCs and their derivatives (Fig. S4A). We identified individual clusters and mapped pseudo-time trajectory for cerebellar lineages (Fig. S4B-D and 3A). scRNAseq analyses suggest that Sox2$^+$ progenitors split into two major lineages: glutamatergic cells from RL and GABAergic cells from VZ, in agreement with lineage tracing (Fig. 3A).

In the *Drosophila* brain, neural progenitors give rise to daughter cells that adopt alternative fates via the Notch pathway [14]. In the mammalian brain, Notch activity is crucial for maintaining neural progenitor state and inhibiting neurogenesis [15] but there is no evidence that neural stem cells use Notch to generate neuronal diversity. We asked whether the expression of Notch pathway genes correlates with cell fate in cerebellar scRNAseq data. We found that Sox2$^+$ progenitors have the highest level of Notch activity, followed by Ptf1a$^+$ VZ precursors, while Atoh1$^+$ RL precursors have the lowest levels of Notch activity, but the highest levels of

Notch ligands Dll1 and Dll3 (Fig.3A, S4E-F, S4I-J, S4N-O, S4K-M, S4P-R and Table 2). This suggests that Notch activity may play a role in successive fate decisions of eCSC: first to segregate eCSCs from their fate-restricted daughters, and then Ptf1a$^+$ PC precursors from Atoh1$^+$ GC precursors.

To test this, we first created Notch gain of function (GOF) eCSC clones using *Sox2*$^{CreERT2/+}$/*Gt(ROSA)26Sor*^{tdTomato}/*R26R*$^{stop\text{-}NICD\text{-}nGFP}$ mice. While both Ptf1a$^+$ and Atoh1$^+$ precursors were significantly reduced, quantification showed that the effect was stronger on Atoh1$^+$ cells than on Ptf1a$^+$ cells (Fig. 3B-J and S5C-G). Conversely, Notch GOF significantly increased Sox2$^+$ eCSCs in the RL and VZ (Fig. 3M-Q, S5E-F'' and S5H), at the expense of both Ptf1a$^+$ and Atoh1$^+$ cells. Thus, constitutive activation of Notch in eCSCs inhibits differentiation into both excitatory and inhibitory fates and retains cells in a Sox2$^+$/Notch^{HIGH} eCSC state.

Next, we asked whether the choice between Ptf1a$^+$ and Atoh1$^+$ cells requires Notch signaling. We examined Notch loss of function (LOF) either in clones using *Sox2*^{CreERT2}/*Notch1*^{flox}/*Atoh1*^{GFP} conditional knockout (KO) mice, or in Presenilin1 KO (Psn1) mice, which have a near-complete loss of Notch activity. Notch1 ablation in eCSC clones increased the number of Sox2$^+$/Atoh1-GFP$^+$ double positive cells and Atoh1$^+$ cells could now be found in the VZ (Fig. 4A-D), indicating Notch LOF induces Sox2$^+$ cells to differentiate into Atoh1$^+$ precursors. The increase in Atoh1$^+$ cells came at the expense of Ptf1a$^+$ cells which were significantly decreased in Notch1 LOF eCSC clones (Fig. 4E-G) as well as Psn1 KO mice (Fig. 4H-J, S7A-B). Importantly, the ratio of the increase in Atoh1$^+$ cells was nearly identical to the ratio of decrease in Ptf1a$^+$ cells (0.672 vs 0.673, Fig. 4G, J). Furthermore, whereas wild type cerebellar precursors rarely co-express Atoh1 and Ptf1a [8], there was a dramatic increase in Ptf1a$^+$/Atoh1$^+$ double positive cells under Notch inactivation conditions (Fig. S6), suggesting a failure in resolving cell fate. Lineage tracing suggested that other types of GABAergic VZ precursors also derive from Sox2$^+$ eCSCs. We examined the expression of other VZ precursor markers, namely Olig2, which maintains the identity of PC progenitors [16], and Lhx1/5, a marker for early GABAergic cells, in Psn KO mice and found that both were decreased, concomitantly with the increase in the number of Atoh1$^+$ cells (Fig. S7C and S7D-H). Therefore, Notch activity regulates the choice of eCSC progeny between excitatory and inhibitory precursor fate.

Discussion

In *Drosophila* neuronal lineages, the two daughter neurons of the same precursor use Notch to adopt different identities during terminal cell division [17–19]. Similarly, spinal cord inhibitory interneurons use Notch activity to adopt different identities [20]. Single cell analysis in the neocortex is beginning to reveal significant diversity of excitatory neuronal fates in the same cortical layers [21]. It would be interesting to test whether Notch signaling is also used to distinguish the fate of excitatory cortical neurons, where paucity of markers may have precluded such findings.

In contrast to text book models, we show that mouse and human cerebellar GABAergic and glutamatergic neurons derive form common progenitors, which we term embryonic Cerebellar Stem Cells. Although we mainly focused on PCs and GCs, lineage tracing showed that eCSCs likely give rise to most cerebellar cells. eCSCs span the RL and the VZ and are characterized by the expression of $Sox2^+$ and high levels of Notch activity. We thus provide mechanistic evidence for how common progenitors can generate both excitatory and inhibitory lineages in the mammalian brain. It will be interesting to test whether Notch activity in eCSCs or their daughters may play a role in disorders of cell fate or stem cell behavior such as medulloblastomas.

Acknowledgemnets

This work was supported by the program "Investissements d'avenir" ANR-10-IAIHU-06, ICM, (to B.A.H.), Armenise-Harvard Foundation, AIRC and CARITRO (to L.T.) and the European Research Council (to S.H.) Work in the Hippenmeyer laboratory was also supported by the under the European Union's Horizon 2020 research and innovation programme (grant agreement No 725780 LinPro) to S.H. T.T.Z., T.Y.L. were supported by doctoral fellowships form the China Scholarship Council and A.H.H. by a doctoral fellowship of the Austrian Academy of Sciences. Light microscopy work was carried out at ICM's imaging core facility, ICM.Quant, and analysis of scRNAseq data was carried out at ICM's bioinofmrtaics core facility, iCONICS. We thank Paulina Ejsmont, Natalia Danda and Nathalie De Geest for technical support. We are grateful to Dr. Shahragim TAJBAKHSH for providing $R26R^{stop\text{-}NICD\text{-}nGFP}$ transgenic mice, Dr. Bart De Strooper for Presenilin1 deficient mice. We also thanks to Dr. Mikio Hoshino for providing Atoh1 and Ptf1a antibodies. B.A.H. is an Allen Distinguished Investigator and an Einstein Visiting Fellow of the Berlin Institute of Health.

Author Contributions

B.A.H. and T.T.Z. designed the project and the experiments and prepared the manuscript with input from S.H. and L.T.; T.T.Z., T.Y.L. performed the majority of mouse experiments and data analysis; X.C., A.H.H., and C.S. performed the MADM experiments supervised by S.H.; M.A. performed the human organoid work supervised by L.T.; N.M. initiated the experimental work; J.G. and M.B. performed bioinformatic analysis.

References

1. Wang, V. Y. & Zoghbi, H. Y. Genetic regulation of cerebellar development. *Nat. Rev. Neurosci.* **2**, 484–491 (2001).
2. du Plessis, A. J., Limperopoulos, C. & Volpe, J. J. Cerebellar Development. *Volpe's Neurol. Newborn* 73–99 (2017). doi:10.1016/B978-0-323-42876-7.00004-1
3. Wagner, M. J. & Luo, L. Neocortex–Cerebellum Circuits for Cognitive Processing. *Trends in Neurosciences* **43**, 42–54 (2020).
4. Manto, M., Gandini, J., Feil, K. & Strupp, M. Cerebellar ataxias: an update. *Curr. Opin. Neurol.* **33**, 150–160 (2020).
5. Northcott, P. A. *et al.* Medulloblastoma. *Nature Reviews Disease Primers* **5**, (2019).
6. Leto, K. *et al.* Consensus Paper: Cerebellar Development. *The Cerebellum* **15**, 789–828 (2016).
7. Vladoiu, M. C. *et al.* Childhood cerebellar tumours mirror conserved fetal transcriptional programs. *Nature* 1 (2019). doi:10.1038/s41586-019-1158-7
8. Yamada, M. *et al.* Specification of spatial identities of cerebellar neuron progenitors by ptf1a and atoh1 for proper production of GABAergic and glutamatergic neurons. *J. Neurosci.* **34**, 4786–800 (2014).
9. Wang, V. Y., Rose, M. F. & Zoghbi, H. Y. Math1 expression redefines the rhombic lip derivatives and reveals novel lineages within the brainstem and cerebellum. *Neuron* **48**, 31–43 (2005).
10. Muguruma, K., Nishiyama, A., Kawakami, H., Hashimoto, K. & Sasai, Y. Self-organization of polarized cerebellar tissue in 3D culture of human pluripotent stem

cells. *Cell Rep.* **10**, 537–550 (2015).

11. Beattie, R. *et al.* Mosaic Analysis with Double Markers Reveals Distinct Sequential Functions of Lgl1 in Neural Stem Cells. *Neuron* **94**, 517-533.e3 (2017).

12. Gao, P. *et al.* Deterministic progenitor behavior and unitary production of neurons in the neocortex. *Cell* **159**, 775–788 (2014).

13. Carter, R. A. *et al.* A Single-Cell Transcriptional Atlas of the Developing Murine Cerebellum. *Curr. Biol.* **28**, 2910-2920.e2 (2018).

14. Bertet, C. *et al.* Temporal patterning of neuroblasts controls notch-mediated cell survival through regulation of hid or reaper. *Cell* **158**, 1173–1186 (2014).

15. Chambers, C. B. *et al.* Spatiotemporal selectivity of response to Notch1 signals in mammalian forebrain precursors. *Development* **128**, 689–702 (2001).

16. Ju, J. *et al.* Olig2 regulates Purkinje cell generation in the early developing mouse cerebellum. *Sci. Rep.* **6**, 30711 (2016).

17. Pinto-Teixeira, F. & Desplan, C. Notch activity in neural progenitors coordinates cytokinesis and asymmetric differentiation. *Sci. Signal.* **7**, pe26 (2014).

18. Artavanis-Tsakonas, S., Rand, M. D. & Lake, R. J. Notch Signaling: Cell Fate Control and Signal Integration in Development. *Science (80-.).* **284**, 770–776 (1999).

19. Bhat, K. M. Notch signaling acts before cell division to promote asymmetric cleavage and cell fate of neural precursor cells. *Sci. Signal.* **7**, ra101 (2014).

20. Peng, C. Y. *et al.* Notch and MAML Signaling Drives Scl-Dependent Interneuron Diversity in the Spinal Cord. *Neuron* **53**, 813–827 (2007).

21. Pfeffer, C. K. & Beltramo, R. Correlating Anatomy and Function with Gene Expression in Individual Neurons by Combining in Vivo Labeling, Patch Clamp, and Single Cell RNA-seq. *Front. Cell. Neurosci.* **11**, (2017).

22. Murtaugh, L. C., Stanger, B. Z., Kwan, K. M. & Melton, D. A. *Notch signaling controls multiple steps of pancreatic differentiation*. *Proceedings of the National Academy of Sciences of the United States of America* **100**, (2003).

23. Butler, A., Hoffman, P., Smibert, P., Papalexi, E. & Satija, R. Integrating single-cell transcriptomic data across different conditions, technologies, and species. *Nat.*

Biotechnol. **36**, 411–420 (2018).

24. Qiu, X. *et al.* Reversed graph embedding resolves complex single-cell trajectories. *Nat. Methods* **14**, 979–982 (2017).

25. Arnold, K. *et al.* Sox2(+) adult stem and progenitor cells are important for tissue regeneration and survival of mice. *Cell Stem Cell* **9**, 317–29 (2011).

26. Hippenmeyer, S. *et al.* Genetic mosaic dissection of Lis1 and Ndel1 in neuronal migration. *Neuron* **68**, 695–709 (2010).

27. Ishida, Y. *et al.* Vulnerability of Purkinje Cells Generated from Spinocerebellar Ataxia Type 6 Patient-Derived iPSCs. *Cell Rep.* **17**, 1482–1490 (2016).

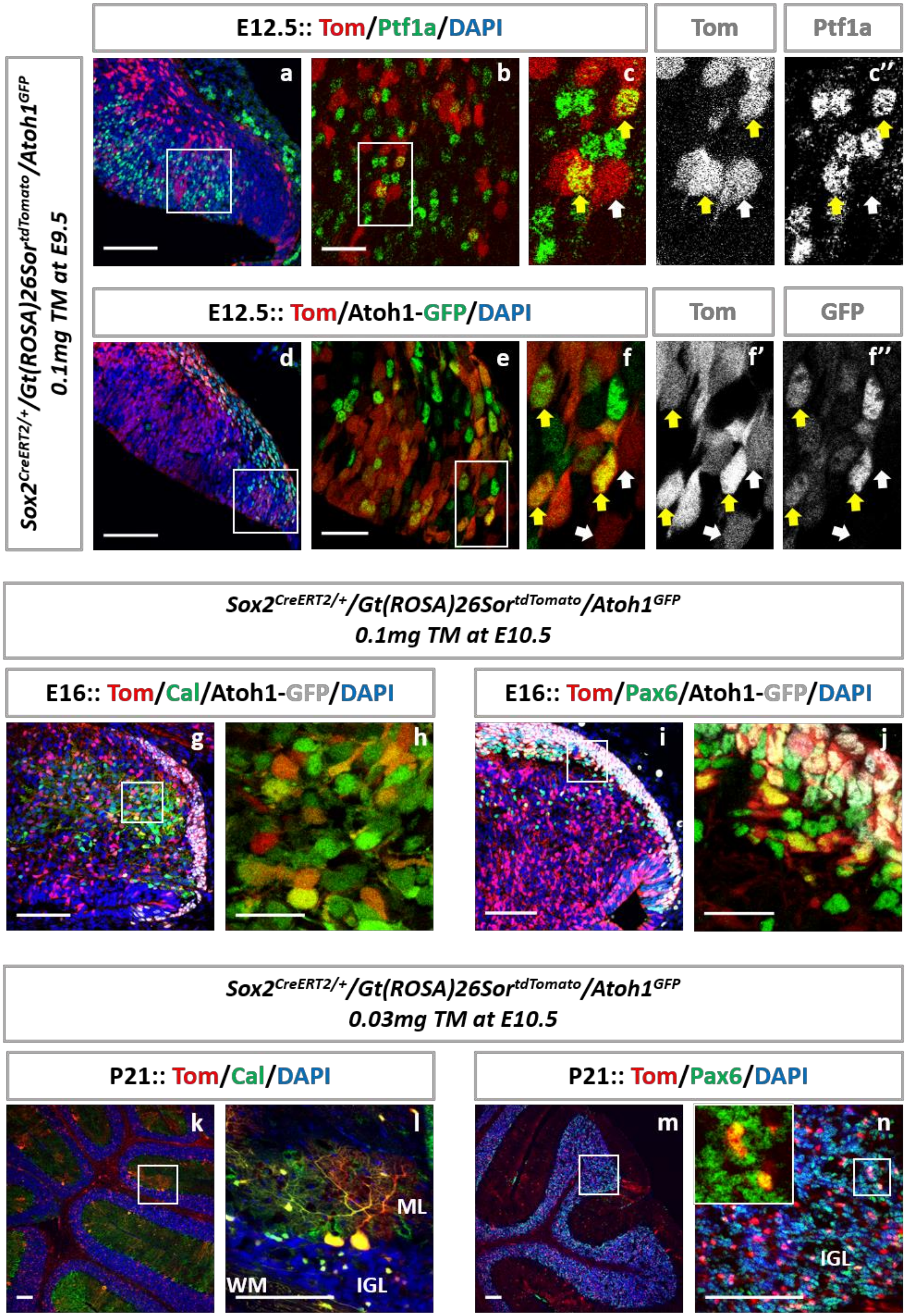
E12.5:: Tom/Ptf1a/DAPI
Tom
Ptf1a
$Sox2^{CreERT2/+}/Gt(ROSA)26Sor^{tdTomato}/Atoh1^{GFP}$
0.1mg TM at E9.5
a
b
c
c'
c''
E12.5:: Tom/Atoh1-GFP/DAPI
Tom
GFP
d
e
f
f'
f''
$Sox2^{CreERT2/+}/Gt(ROSA)26Sor^{tdTomato}/Atoh1^{GFP}$
0.1mg TM at E10.5
E16:: Tom/Cal/Atoh1-GFP/DAPI
E16:: Tom/Pax6/Atoh1-GFP/DAPI
g
h
i
j
$Sox2^{CreERT2/+}/Gt(ROSA)26Sor^{tdTomato}/Atoh1^{GFP}$
0.03mg TM at E10.5
P21:: Tom/Cal/DAPI
P21:: Tom/Pax6/DAPI
k
l
ML
WM
IGL
m
n
IGL

Fig. 1 Lineage tracing of eCSCs

(A-B) Co-localization of Ptf1a (green) and tdTomato (red) in VZ at E12.5. (C-C'') High magnification of the rectangle in (B). (D-E) Co-localization of Atoh1 (green) and tdTomato (red) in RL at E12.5. (F-F'') High magnification of the rectangle in (E). (G-N) Co-localization of tdTomato (red) with Calbindin$^+$ (green, G,H,K,L) or Pax6$^+$ (green, I,J,M,N) at E16 and P21. (H,J,L,N) High magnification of the rectangles. Nuclei marked with DAPI (blue). Yellow arrows indicate double-positive cells (tdTomato/Ptf1a or Atoh1-GFP), white arrows indicate tdTomato-only cells. Scalebars=100μm and 25μm.

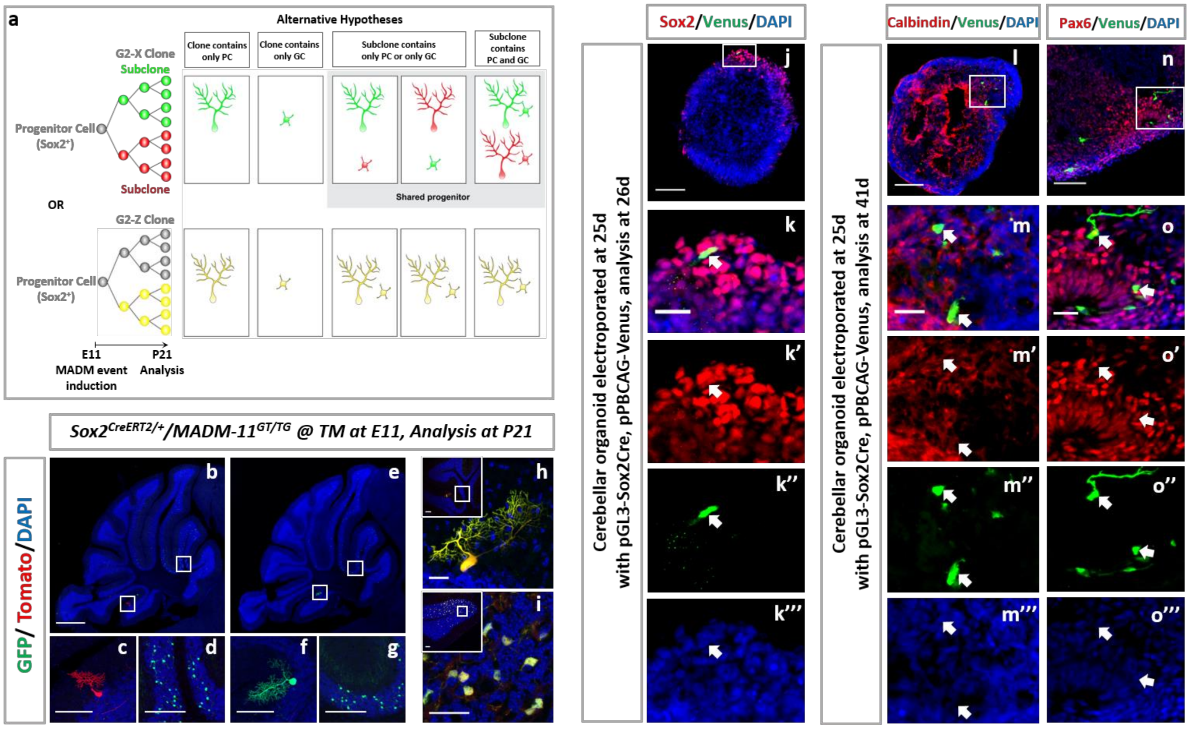
a
Alternative Hypotheses
Clone contains only PC
Clone contains only GC
Subclone contains only PC or only GC
Subclone contains PC and GC
G2-X Clone
Subclone
Progenitor Cell (Sox2+)
Subclone
Shared progenitor
OR
G2-Z Clone
Progenitor Cell (Sox2+)
E11 MADM event induction
P21 Analysis
Sox2CreERT2/+/MADM-11GT/TG @ TM at E11, Analysis at P21
GFP/ Tomato/DAPI
b
c
d
e
f
g
h
i
Sox2/Venus/DAPI
Cerebellar organoid electroporated at 25d with pGL3-Sox2Cre, pPBCAG-Venus, analysis at 26d
j
k
k'
k''
k'''
Calbindin/Venus/DAPI
Pax6/Venus/DAPI
Cerebellar organoid electroporated at 25d with pGL3-Sox2Cre, pPBCAG-Venus, analysis at 41d
l
m
m'
m''
m'''
n
o
o'
o''
o'''

Fig. 2 Sparse lineage tracing of eCSCs in the mouse and in human cerebellar organoids

(A) Scheme of MADM-clones at E11 in *MADM-11*$^{GT/TG}$/*Sox2*^{CreER} mice. (B,E) Sparse G2-X MADM clones at P21. Two PCs (red and green) and tens of GCs (green) were found in the same cerebellum. Scalebars=500µm. (C,D,F,G) High magnification of the rectangle in (B,E). Scalebars=25µm. (H-I) Sparse G2-Z MADM clones at P21 cerebellum. One PC (H, yellow) and tens of GCs (I, yellow) were found in two cerebella. Scalebar=25µm. (J) Expression of Venus (green) and Sox2 (red) 1 day after electroporation. (K-K''') Higher magnification of the rectangle in (J). Arrows indicate Sox2^{+}/Venus^{+} cells. (L-N) 16 post-electroporation both PC marker (Calbindin, red) or GC marker (Pax6, red) co-localized with Venus (green). (M-M''', O-O''') Higher magnification of the rectangle in (L,N). Scalebars=100µm and 25µm. Nuclei marked with DAPI (blue).

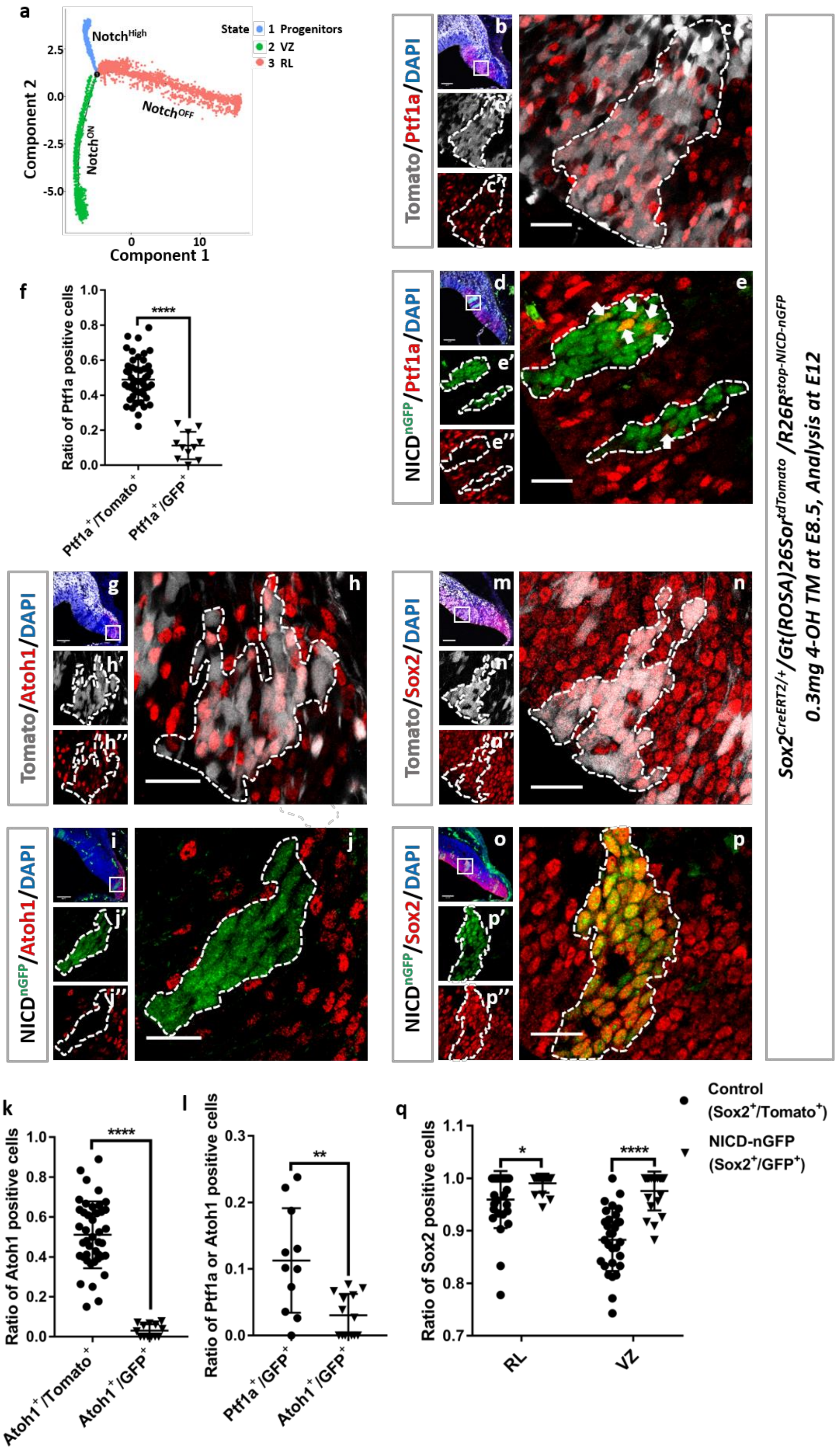
a
State
1 Progenitors
2 VZ
3 RL
Notch^High
Notch^ON
Notch_OFF
Component 1
Component 2
2.5
0.0
-2.5
-5.0
0
10
b
c
c'
c''
Tomato/Ptf1a/DAPI
d
e
e'
e''
NICD^nGFP/Ptf1a/DAPI
Sox2^CreERT2/+/Gt(ROSA)26Sor^tdTomato/R26R^stop-NICD-nGFP
0.3mg 4-OH TM at E8.5, Analysis at E12
f
Ratio of Ptf1a positive cells
1.0
0.8
0.6
0.4
0.2
0.0
****
Ptf1a+/Tomato+
Ptf1a+/GFP+
g
h
h'
h''
Tomato/Atoh1/DAPI
m
n
n'
n''
Tomato/Sox2/DAPI
i
j
j'
j''
NICD^nGFP/Atoh1/DAPI
o
p
p'
p''
NICD^nGFP/Sox2/DAPI
k
Ratio of Atoh1 positive cells
1.0
0.8
0.6
0.4
0.2
0.0
****
Atoh1+/Tomato+
Atoh1+/GFP+
l
Ratio of Ptf1a or Atoh1 positive cells
0.3
0.2
0.1
0.0
**
Ptf1a+/GFP+
Atoh1+/GFP+
q
Ratio of Sox2 positive cells
1.1
1.0
0.9
0.8
0.7
*
****
RL
VZ
● Control (Sox2+/Tomato+)
▼ NICD-nGFP (Sox2+/GFP+)

Fig. 3 Notch GOF in eCSCs

(A) Pseudo-time trajectory of scRNAseq data in the E10-E13 cerebellum: eCSCs (blue), VZ GABAergic lineages (green) and RL glutamatergic lineages (red). (B) Immunostaining for Ptf1a^{+} (red) in tdTomato^{+} wildtype clones (grey) at E12. (C-C'') Higher magnification of the rectangle in (B). (D) Immunostaining for Ptf1a^{+} (red) in NICD-GFP^{+} clones (green) at E12. (E-E'') Higher magnification of the rectangle in (D). Arrows indicate NICD-GFP^{+}/Ptf1a^{+} double-positive cells. (F) Percentage of Ptf1a^{+} cells in control (tdTomato^{+}) versus NICD-GFP^{+} VZ clones. (G) Immunostaining for Atoh1^{+} (red) in tdTomato^{+} wildtype clones (grey) at E12. (H-H'') Higher magnification of the rectangle in (G). (I) Immunostaining for Atoh1^{+} (red) in NICD-GFP^{+} clones (green) at E12. (J-J'') Higher magnification of the rectangle in (I). (K) Percentage of Atoh1^{+} cells in control (tdTomato^{+}) versus NICD-GFP^{+} RL clones. (L) Comparison of the ratios of Ptf1a^{+} cells and Atoh1^{+} cells in NICD-GFP^{+} clones. (M) Immunostaining for Sox2^{+} (red) in tdTomato^{+} wildtype clones (grey) at E12. (N-N'') Higher magnification of the rectangle in (M). (O) Immunostaining for Sox2^{+} (red) in NICD-GFP^{+} clones at E12. (P-P'') Higher magnification of the rectangle in (O). (Q) Percentage of Sox2^{+} cells in in control (tdTomato^{+}) versus NICD-GFP^{+} RL and VZ clones. Nuclei marked with DAPI (blue). Scalebars=100 μm and 25 μm. Data distribution is mean ± SD. *$p < 0.05$; **$p < 0.01$; ****$p < 0.0001$.

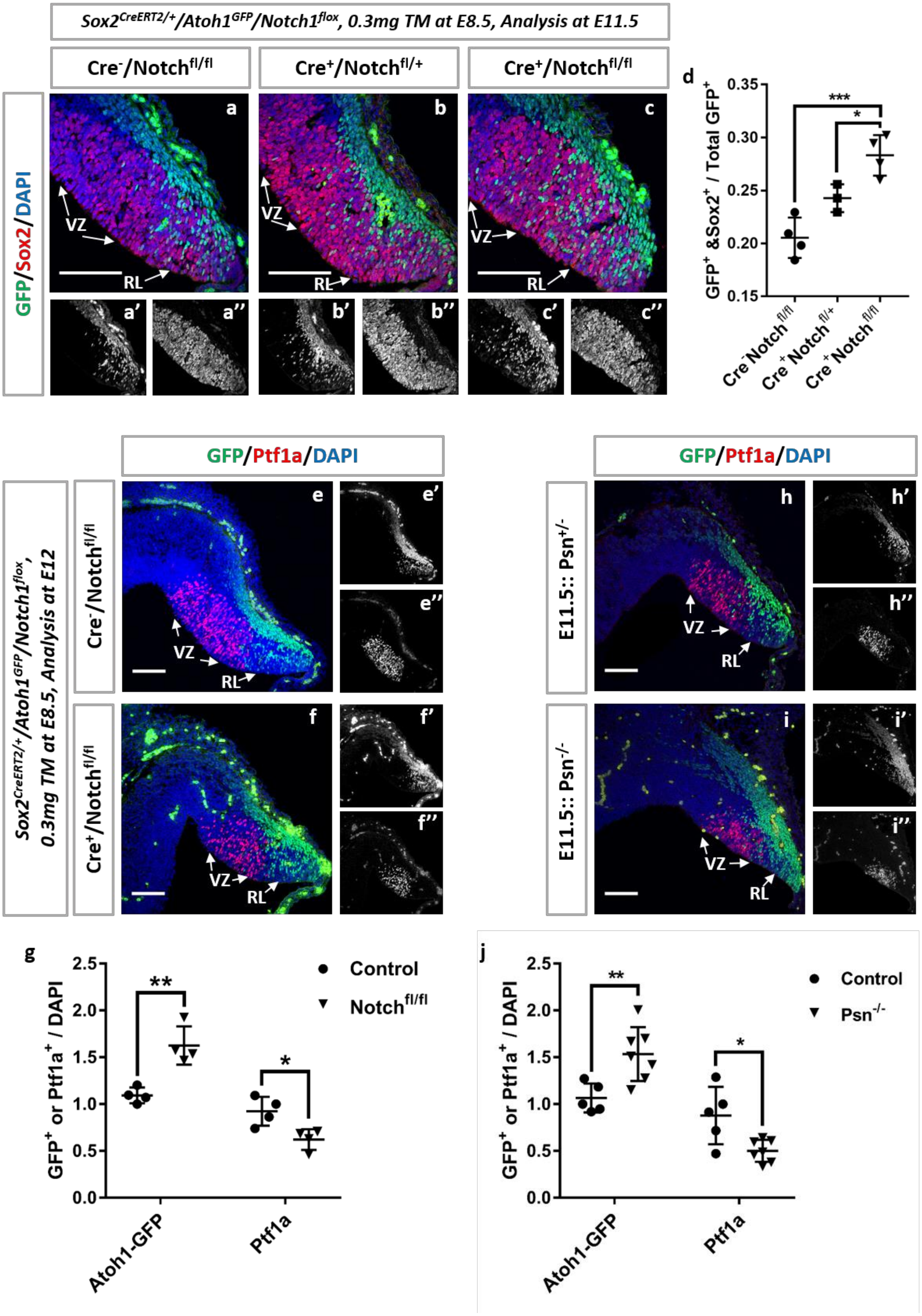

Sox2CreERT2/+/Atoh1GFP/Notch1flox, 0.3mg TM at E8.5, Analysis at E11.5
Cre-/Notchfl/fl
Cre+/Notchfl/+
Cre+/Notchfl/fl
GFP/Sox2/DAPI
a
b
c
VZ
RL
a'
a''
b'
b''
c'
c''
d
GFP+ &Sox2+ / Total GFP+
0.35
0.30
0.25
0.20
0.15
***
*
Cre-Notchfl/fl
Cre+Notchfl/+
Cre+Notchfl/fl
GFP/Ptf1a/DAPI
Sox2CreERT2/+/Atoh1GFP/Notch1flox, 0.3mg TM at E8.5, Analysis at E12
Cre-/Notchfl/fl
Cre+/Notchfl/fl
e
e'
e''
f
f'
f''
E11.5:: Psn+/-
E11.5:: Psn-/-
h
h'
h''
i
i'
i''
g
GFP+ or Ptf1a+ / DAPI
2.5
2.0
1.5
1.0
0.5
0.0
**
*
Control
Notchfl/fl
Atoh1-GFP
Ptf1a
j
GFP+ or Ptf1a+ / DAPI
2.5
2.0
1.5
1.0
0.5
0.0
**
*
Control
Psn-/-
Atoh1-GFP
Ptf1a

Fig. 4 Notch loss of function in cerebellar progenitors

(A-C'') Immunostaining for Sox2$^+$ (red) and Atoh1-GFP$^+$ (green) at E11.5 in Cre$^-$/Notch$^{fl/fl}$, Cre$^+$/Notch$^{fl/+}$ and Cre$^+$/Notch$^{fl/fl}$ mice. (D) Percentage of Atoh1-GFP$^+$/Sox2$^+$ double-positive cells within all Atoh1-GFP$^+$ cells in the three genotypes. (E-F'') Immunostaining for Ptf1a$^+$ (red) and Atoh1-GFP$^+$ (green) at E12 in control cerebella (E-E'') and in Notch1 conditional KO (cKO) cerebellum (F-F''). (G) Percentage of Ptf1a$^+$ cells or Atoh1-GFP$^+$ cells within all cells (DAPI, blue) in control and Notch1 cKO cerebellum. (H-I'') Immunostaining for Ptf1a$^+$ (red) and Atoh1-GFP$^+$ cells (green) at E11.5 in Control (H-H'') and Presenilin1 (Psn) KO cerebellum (I-I''). (J) Percentage of Ptf1a$^+$ cells or Atoh1-GFP$^+$ cells within all cells (DAPI) in control and Psn KO cerebellum. Scalebars=100 µm and 25 µm. Data distribution is mean ± SD. $^*p < 0.05$; $^{**}p < 0.01$; $^{***}p < 0.001$.

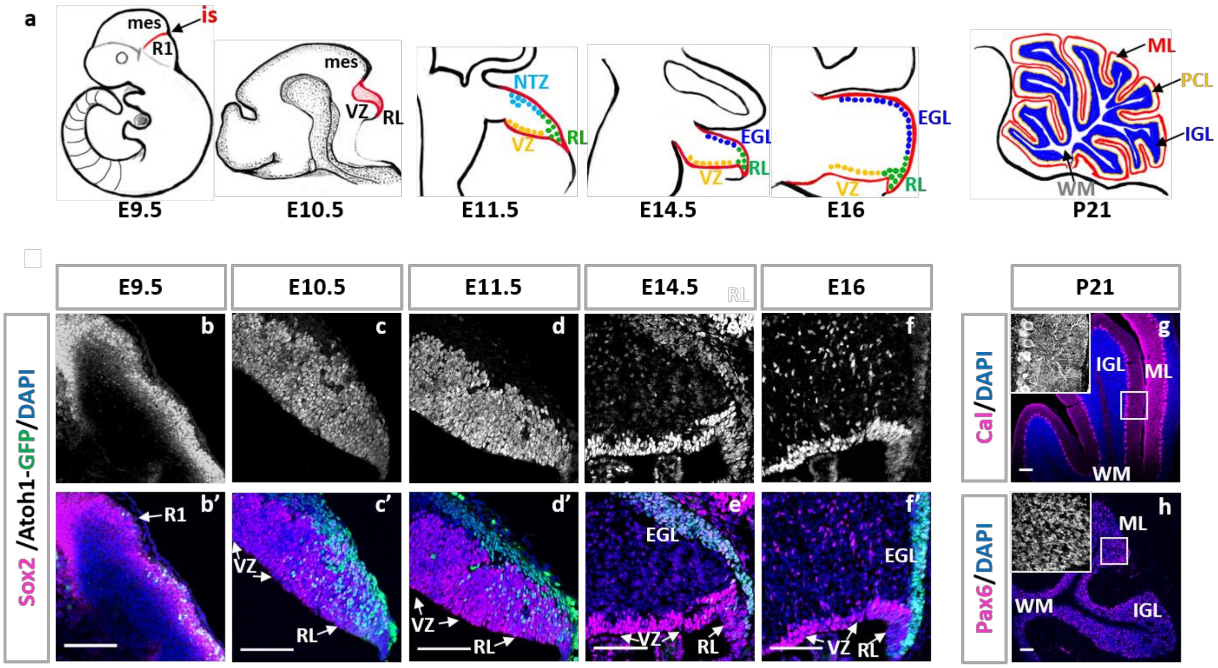
a
mes
is
R1
E9.5
mes
VZ
RL
E10.5
NTZ
VZ
RL
E11.5
EGL
VZ
RL
E14.5
EGL
VZ
RL
E16
ML
PCL
IGL
WM
P21
E9.5
E10.5
E11.5
E14.5
E16
P21
Sox2 /Atoh1-GFP/DAPI
b
c
d
e
f
R1
b'
c'
VZ
RL
d'
VZ
RL
e'
EGL
VZ
RL
f'
EGL
VZ
RL
Cal/DAPI
g
IGL
ML
WM
Pax6/DAPI
h
ML
WM
IGL

Fig. S1 Sox2 is highly expressed in the cerebellar primordium

(A) Cerebellar morphology at different stages during development from E9.5 to P21. R1, rhombomere1; RL, rhombic lip; VZ, ventricular zone; NTZ, nuclear transitory zone; EGL, external granule layer; IGL, internal granule layer; PCL, Purkinje cell layer; ML, molecular layer; WM, white matter. (B-F') Immunostaining for Sox2 (magenta) expression in a time series of mouse cerebellum during development. (G-H) Immunostaining for Calbindin and Pax6 (magenta) expression in the cerebellum at P21. Nuclei were stained with DAPI (blue). Scalebars=100 µm.

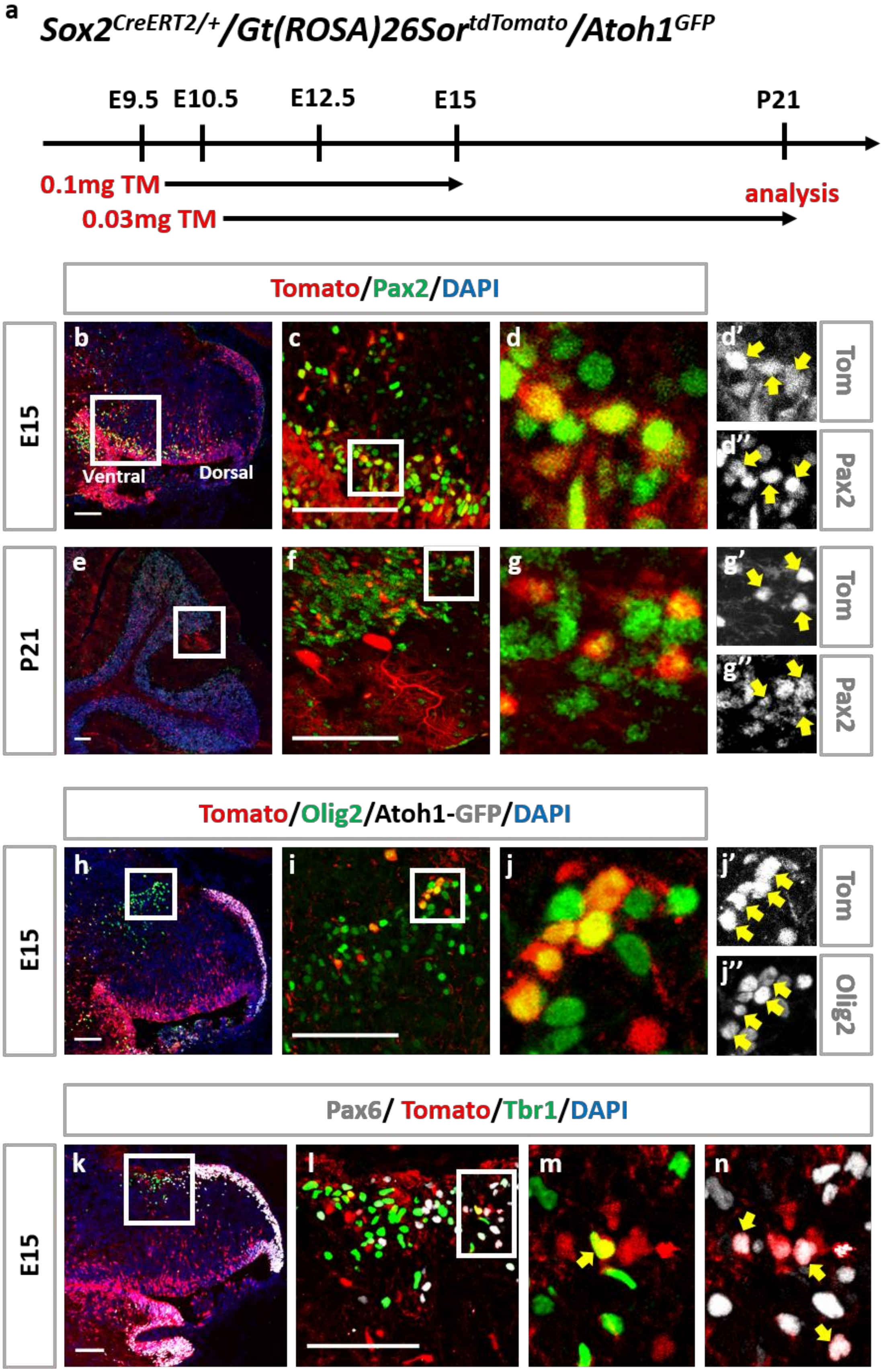
a
$Sox2^{CreERT2/+}/Gt(ROSA)26Sor^{tdTomato}/Atoh1^{GFP}$
E9.5
E10.5
E12.5
E15
P21
0.1mg TM
0.03mg TM
analysis
Tomato/Pax2/DAPI
E15
b
Ventral
Dorsal
c
d
d'
Tom
d''
Pax2
P21
e
f
g
g'
Tom
g''
Pax2
Tomato/Olig2/Atoh1-GFP/DAPI
E15
h
i
j
j'
Tom
j''
Olig2
Pax6/ Tomato/Tbr1/DAPI
E15
k
l
m
n

Fig. S2 Tracing of INs and DCN lineages in the cerebellum

(A) Scheme of the experiments. Pregnant females were injected Tamoxifen at E9.5 or E10.5 through intraperitoneal (i.p.), and the samples were collected at E15 or P21, followed by immunostaining. (B-C) Co-localization of Pax2$^+$ (green, a marker for INs) and Tom$^+$ (red) in cerebellar primordium at E15. (D-D'') Higher magnification of the rectangular region in (C). (E-F) Co-localization of Pax2$^+$ (green) and Tom$^+$ (red) at P21. (G-G'') Higher magnification of the rectangular region in (F). (H-I) Co-localization of Olig2$^+$ (green, a marker for glu-DCN) and Tom$^+$ (red) at E15. (J-J'') Higher magnification of the rectangular region in (I). (K-L) Triple immunolabeling with Tom (red), Pax6 (grey) and Tbr1 (green, a marker for glu-DCN) at E15. (M-N) Higher magnification of the rectangular region in (L). Nuclei were stained with DAPI (blue). Arrows indicate double positive cells of Tom$^+$ with Pax2$^+$ or Olig2$^+$ or Pax6$^+$ or Tbr1$^+$. Scalebars=100 μm and 25 μm.

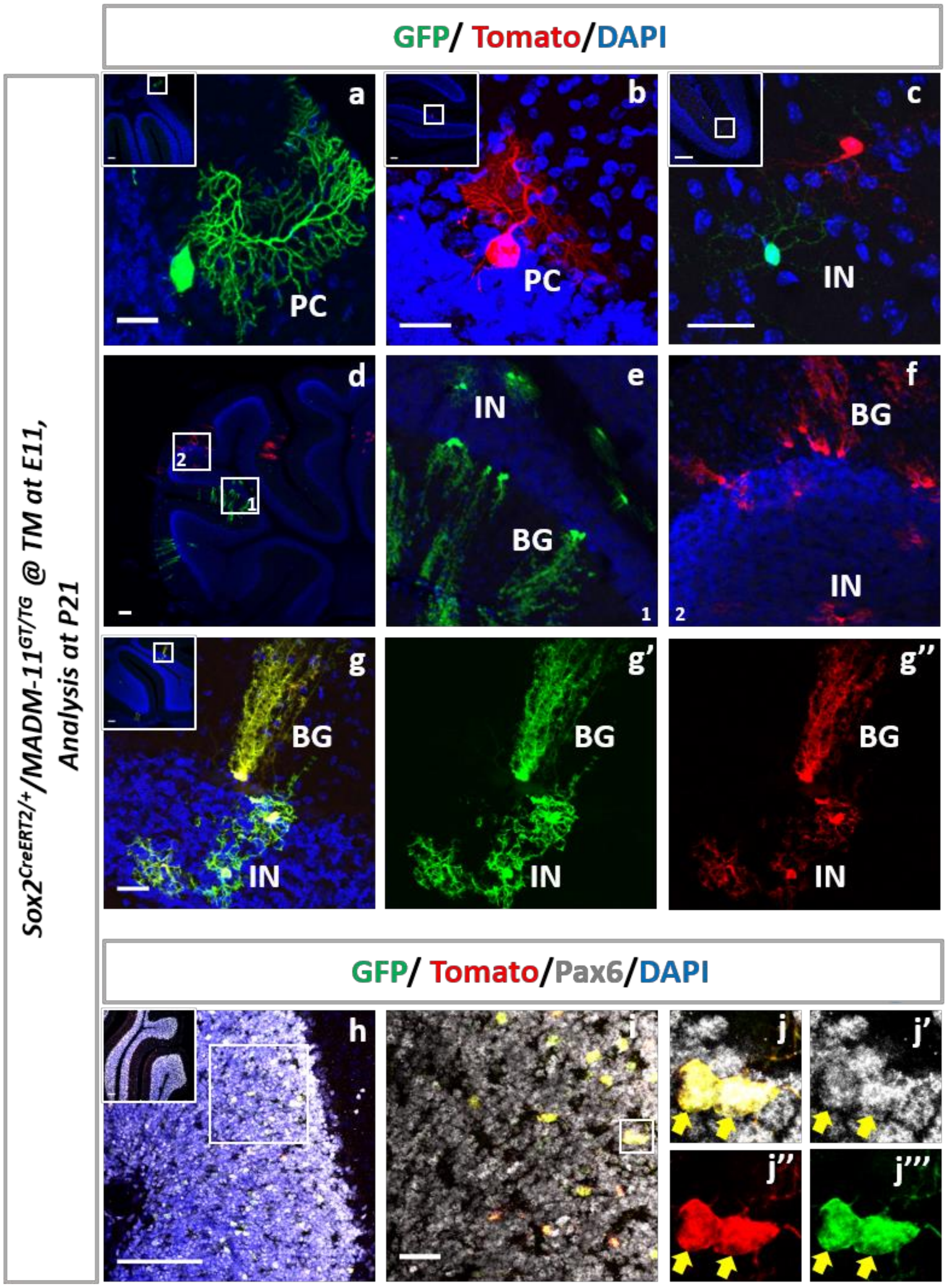
GFP/ Tomato/DAPI
Sox2CreERT2/+/MADM-11GT/TG @ TM at E11, Analysis at P21
a
PC
b
PC
c
IN
d
2
1
e
IN
BG
1
f
BG
IN
2
g
BG
IN
g'
BG
IN
g''
BG
IN
GFP/ Tomato/Pax6/DAPI
h
i
j
j'
j''
j'''

Fig. S3 Tracing of cerebellar lineages using MADM

(A-F) Sparse G2-X MADM labeling cells in P21 cerebellum. Two PCs (red and green), several Interneurons (Ins, green and red) and Bergmann glia were found in different mouse cerebella. (G-G'') Sparse G2-Z MADM labeling cells in P21 cerebellum. Several yellow INs and Bergmann glia were found in mouse cerebella. (H-I) Immunostaining for Pax6, a marker for GCs, at P21. (J-J''') Higher magnification of the rectangular region in (E). Nuclei were stained with DAPI (blue). Scalebars=100 µm and 25 µm.

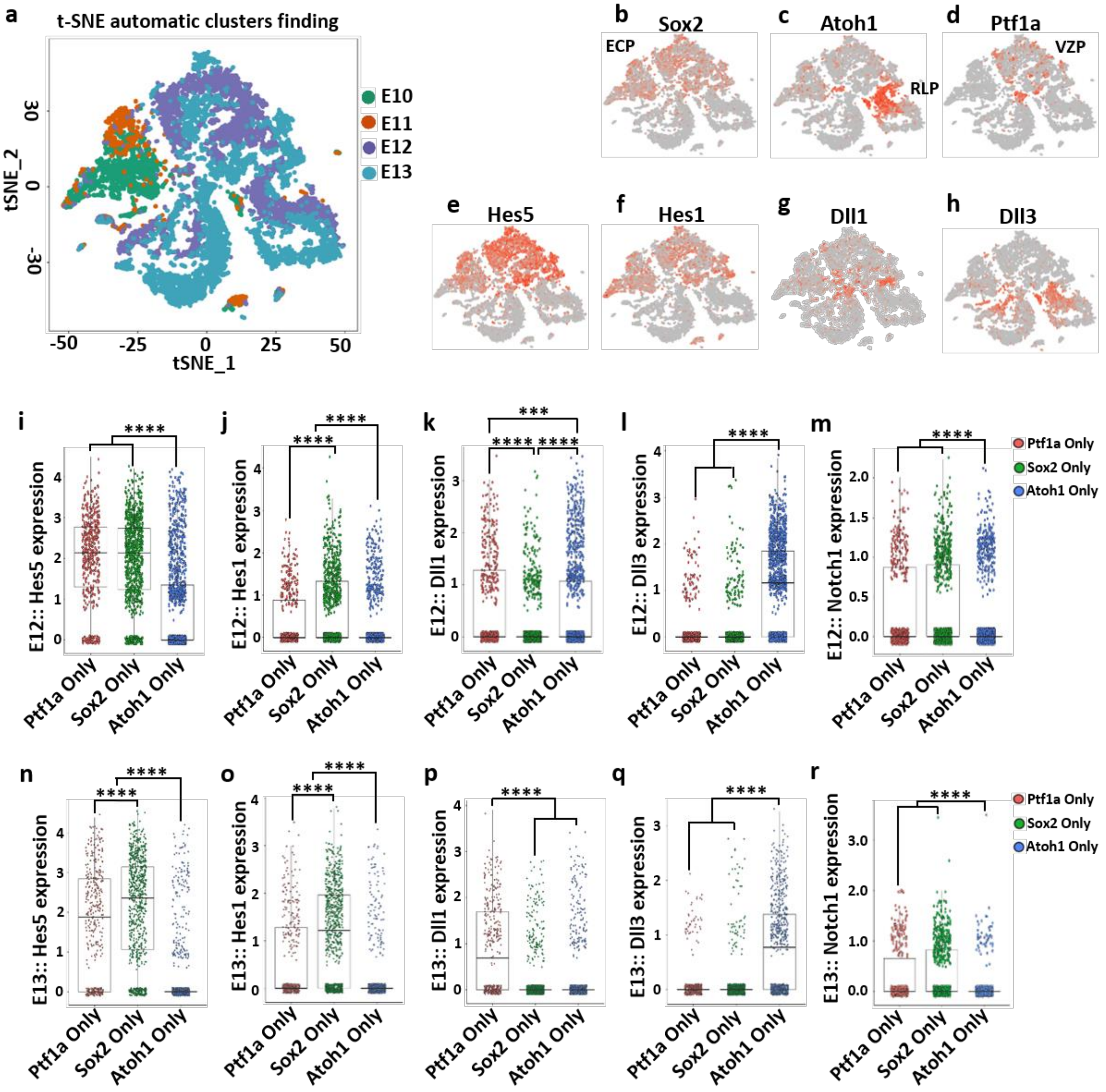

Fig. S4 Analysis of Notch signaling gene expression in scRNAseq data from embryonic cerebellar progenitors

(A) t-distributed stochastic neighbor embedding (t-SNE) visualizations of cerebellar derived cell clusters (right) and developmental time points (left) at E10-E13. Each point represents one cell. (B-D) t-SNE shows cell type specific markers expression: Sox2, Atoh1 and Ptf1a. ECPs, Embryonic Cerebellar Progenitors; RLP, rhombic lip progenitors; VZP, ventricular zone progenitors. Cells are color-coded according to genes expression. (E-H) t-SNE shows Notch signaling related genes expression: Hes5, Hes1, Dll1 and Dll3. Cells are color-coded according to genes expression. (I-R) Expression of Hes5, Hes1, Dll1, Dll3 and Notch1 in three different groups: Ptf1a only, Sox2 only and Atoh1 only both at E12 (I-M) and E13 (N-R). Box plot center lines are median. ***$p < 0.001$, ****$p < 0.0001$.

Table 2. scRNAseq analysis of the mean level of Notch signaling related genes at E12 and E13

	Ptf1a only		Sox2 only		Atoh1 only	
	E12	E13	E12	E13	E12	E13
Number of cells	479	370	898	975	1375	665
Mean (Hes5)	2.0106	1.7200	1.9952	2.1000	1.1337	0.5000
Mean (Hes1)	0.4288	0.6121	0.6756	1.1664	0.3307	0.2595
Mean (Notch1)	0.3358	0.3026	0.3659	0.3639	0.2625	0.0847
Mean (Dll1)	0.6101	0.8748	0.3115	0.2302	0.5419	0.3557
Mean (Dll3)	0.2110	0.1502	0.1325	0.1115	0.8623	0.7710
Mean (Dll4)	0.0012	0.0049	0.0022	0.0050	0.0042	0.0172
Mean (Jag1)	0.0218	0.0241	0.0264	0.0390	0.0328	0.0336
Mean (Jag2)	0	0	0.0007	0	0.0011	0

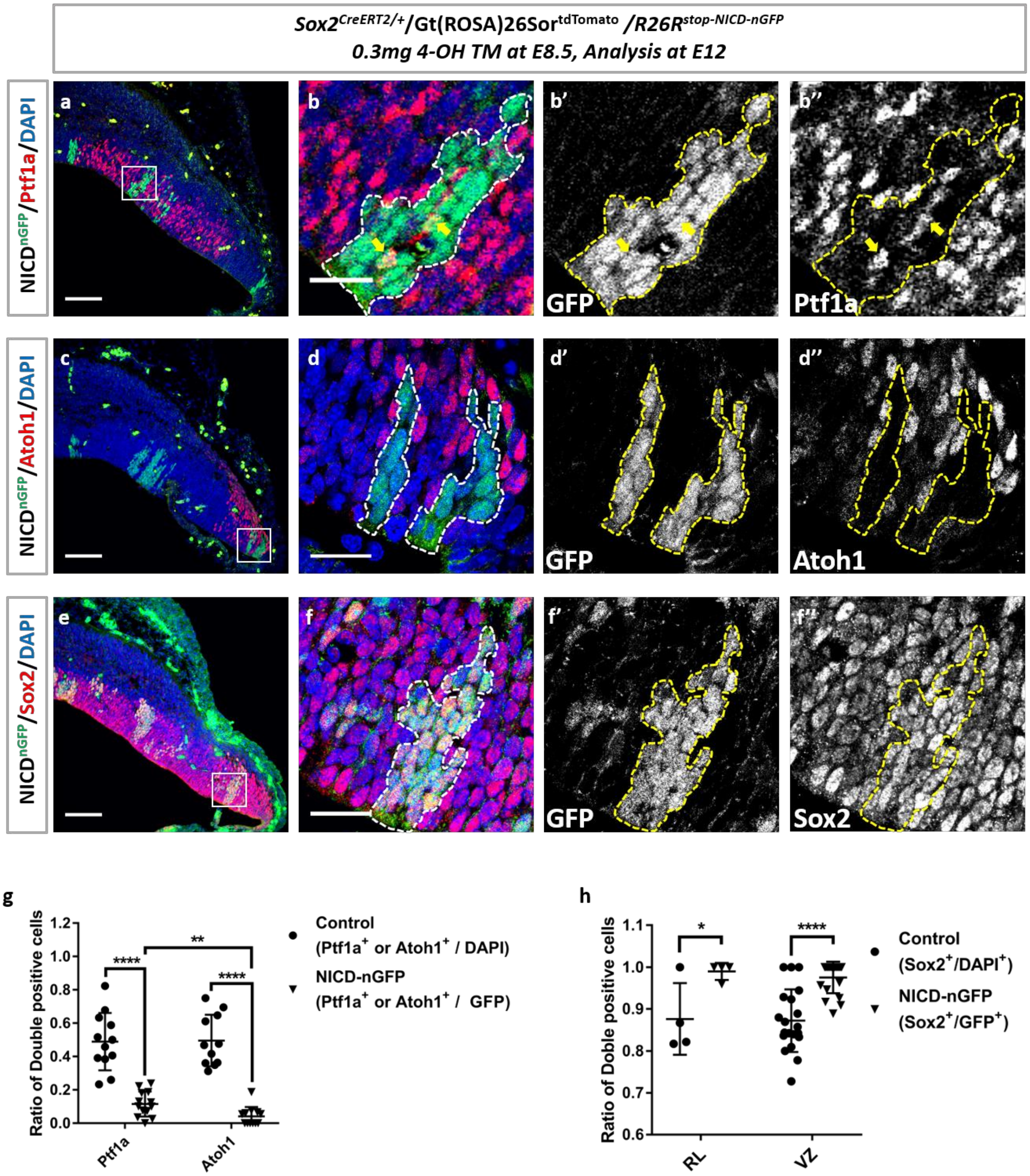

Sox2CreERT2/+/Gt(ROSA)26SortdTomato /R26Rstop-NICD-nGFP
0.3mg 4-OH TM at E8.5, Analysis at E12
NICDnGFP/Ptf1a/DAPI
a
b
b'
b''
GFP
Ptf1a
NICDnGFP/Atoh1/DAPI
c
d
d'
d''
GFP
Atoh1
NICDnGFP/Sox2/DAPI
e
f
f'
f''
GFP
Sox2
g
Ratio of Double positive cells
1.2
1.0
0.8
0.6
0.4
0.2
0.0
****
**
****
Ptf1a
Atoh1
● Control
(Ptf1a+ or Atoh1+ / DAPI)
▼ NICD-nGFP
(Ptf1a+ or Atoh1+ / GFP)
h
Ratio of Doble positive cells
1.1
1.0
0.9
0.8
0.7
0.6
*
****
RL
VZ
● Control
(Sox2+/DAPI+)
▼ NICD-nGFP
(Sox2+/GFP+)

Fig. S5 Effects of Notch gain of function on cerebellar progenitor fate decisions compared to adjacent wild-type cells

(A) Immunostaining for Ptf1a^{+} (red) in GFP^{+} Notch GOF clones (green) at E12. (B-B'') Higher magnification of the rectangular region in (A). Arrows indicate NICD-GFP^{+}/Ptf1a^{+}double positive cells. (C) Immunostaining for Atoh1^{+} (red) in GFP^{+} Notch GOF clones (green) at E12. (D-D'') Higher magnification of the rectangular region in (C). (E) Immunostaining for Sox2^{+} (red) in GFP^{+} Notch GOF clones (green) at E12. (F-F'') Higher magnification of the rectangular region in (A). (G) The ratio of Ptf1a^{+} cells or Atoh1^{+} cells to total cells in GFP^{+} Notch GOF clones (Ptf1a^{+} or Atoh1^{+}/ GFP^{+}) compared to the ratio of Ptf1a^{+} cells or Atoh1^{+} cells to an equivalent number of adjacent control cells (Ptf1a^{+} or Atoh1^{+}/ DAPI^{+}) in the VZ or RL, respectively. (H) The ratio of Sox2^{+} cells to total cells in GFP^{+} Notch GOF clones (Sox2^{+}/GFP^{+}) compared with the ratio of Sox2^{+} cells to an equivalent number of adjacent control cells (Sox2^{+} / DAPI^{+}) both in the RL and VZ. Nuclei were stained with DAPI (blue). Scalebars=100 μm and 25 μm. Data presented as mean ± SD. $^{*}p < 0.05$; $^{**}p < 0.01$; $^{****}p < 0.0001$.

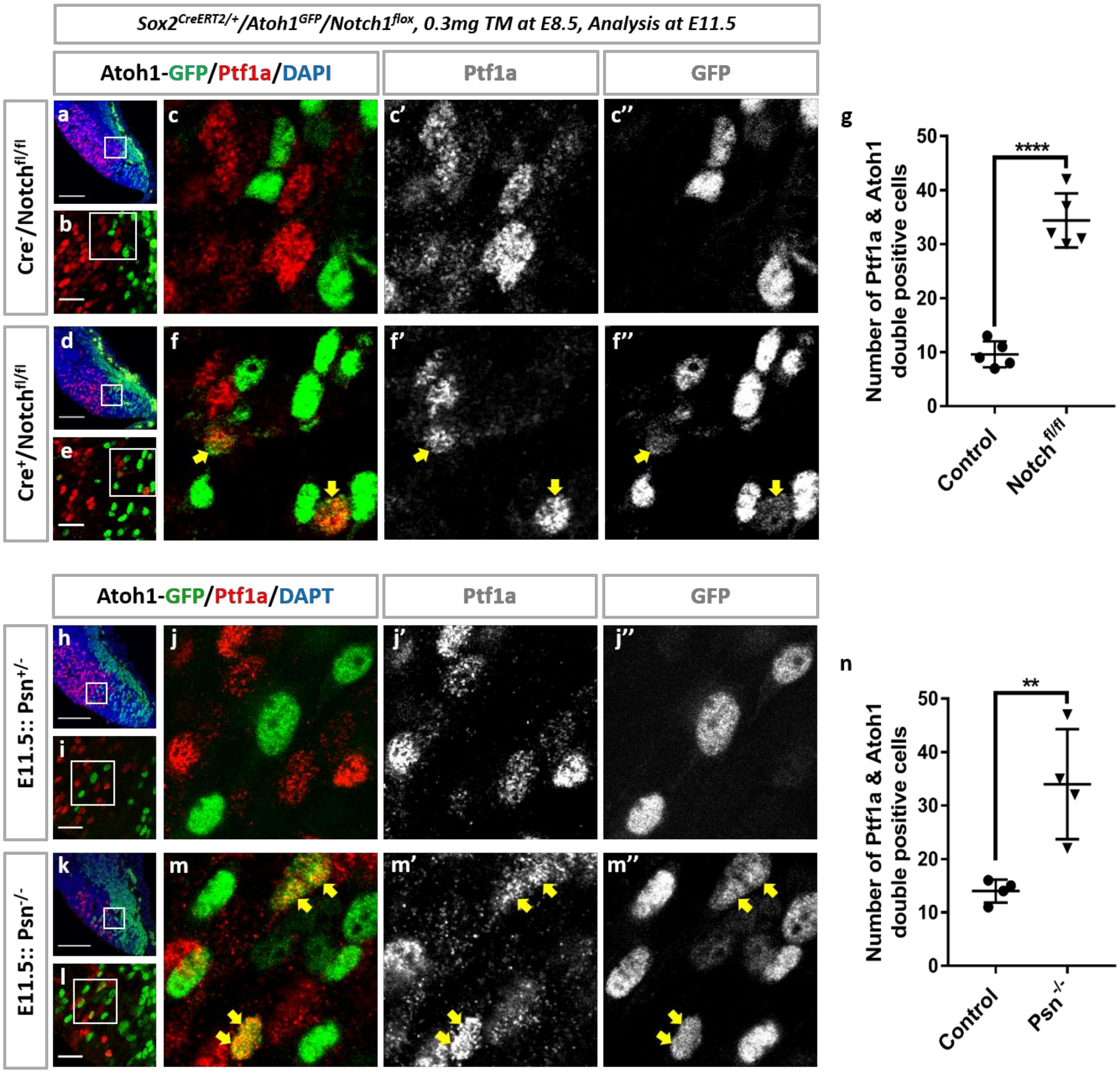
Sox2CreERT2/+/Atoh1GFP/Notch1flox, 0.3mg TM at E8.5, Analysis at E11.5
Atoh1-GFP/Ptf1a/DAPI
Ptf1a
GFP
Cre-/Notchfl/fl
Cre+/Notchfl/fl
a
b
c
c'
c''
d
e
f
f'
f''
g
Number of Ptf1a & Atoh1 double positive cells
50
40
30
20
10
0
****
Control
Notch fl/fl
Atoh1-GFP/Ptf1a/DAPT
Ptf1a
GFP
E11.5:: Psn+/-
E11.5:: Psn-/-
h
i
j
j'
j''
k
l
m
m'
m''
n
Number of Ptf1a & Atoh1 double positive cells
50
40
30
20
10
0
**
Control
Psn -/-

Fig. S6 Notch loss of function increases Ptf1a and Atoh1 double positive cells at the of VZ-RL boundary

(A-B) Immunostaining for Ptf1a$^+$ (red) and Atoh1-GFP$^+$ (green) reveals very few double positive cells at E11.5 in Control cerebellum. (C-C'') Higher magnification of the rectangular region in (B). (D-E) Immunostaining for Ptf1a$^+$ (red) and Atoh1-GFP$^+$ (green) reveals many double positive cells at E11.5 in Notch1 cKO cerebellum. (F-F'') Higher magnification of the rectangular region in (E). Arrows indicate Ptf1a$^+$ and Atoh1-GFP$^+$ double positive cells. (G) Percentage of Ptf1a$^+$ and Atoh1-GFP$^+$ double positive cells in Control and Notch1 cKO cerebellum. (H-I) Immunostaining for Ptf1a$^+$ (red) and Atoh1-GFP$^+$ (green) double positive cells at E11.5 in Control cerebellum. (J-J'') Higher magnification of the rectangular region in (I). (K-L) Immunostaining for Ptf1a$^+$ (red) and Atoh1-GFP$^+$ (green) double positive cells at E11.5 in Psn KO cerebellum. (M-M'') Higher magnification of the rectangular region in (L). Arrows indicate Ptf1a$^+$ and Atoh1-GFP$^+$ double positive cells. (N) Percentage of Ptf1a$^+$ and Atoh1-GFP$^+$ double positive cells in Control and Psn KO cerebellum. Nuclei were stained with DAPI (blue). Scalebars=100 μm and 25 μm. Data presented as mean ± SD. $^{**}p < 0.01$, $^{****}p < 0.0001$.

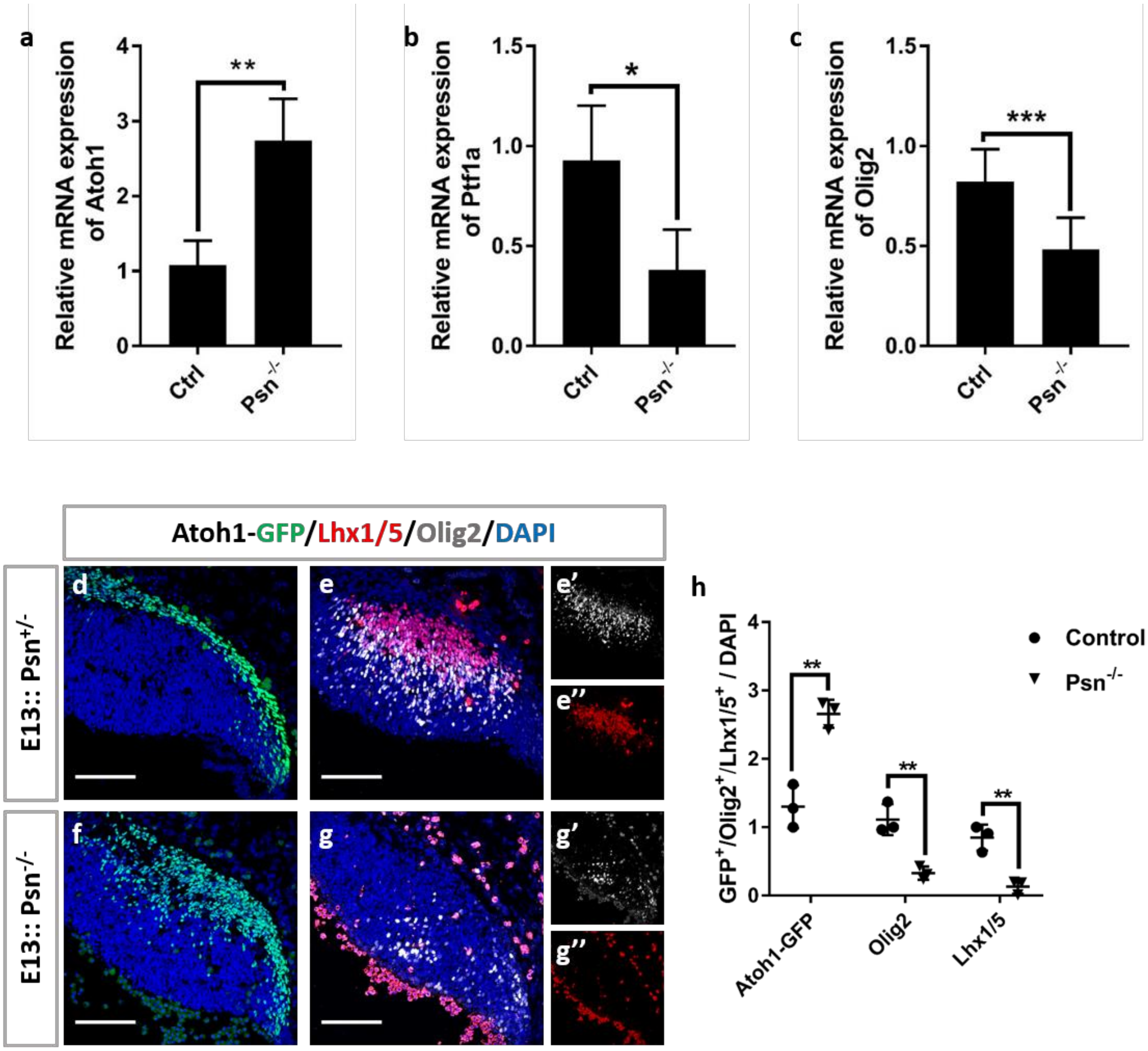

Fig. S7 Notch loss of function increases RL precursors at the expense of VZ precursors

(A-C) Comparison of Atoh1, Ptf1a and Olig2 mRNA levels in Control and Psn KO cerebellum using RT-PCR at E13. (D) Immunostaining for Atoh1-GFP$^+$ cells (green) at E13 in wild-type cerebellum. (E-E'') Immunostaining for Lhx1/5$^+$ cells (red) and Olig2$^+$ (grey) at E13 in Control cerebellum. (F) Immunostaining for Atoh1-GFP$^+$ cells (green) at E13 in Psn KO cerebellum. (G-G'') Immunostaining for Lhx1/5$^+$ cells (red) and Olig2$^+$ (grey) at E13 in Psn KO cerebellum. (H) Percentage of Atoh1-GFP$^+$ cells or Lhx1/5$^+$ cells or Olig2$^+$ cells compared with DAPI in Control and Psn KO cerebellum. Nuclei were stained with DAPI (blue). Scalebars=100 μm. Data presented as mean ± SD. $^*p < 0.05$; $^{**}p < 0.01$; $^{***}p < 0.001$.

Supplementary Materials for

Generation of neuronal diversity from common progenitors via Notch signaling in the cerebellum

Zhang et al.

Materials and Methods

Mice

All animal experiments in this study were carried out in accordance with animal welfare regulations and have been approved by Ethic Committee and French regulatory authorities of the respective institutes. The *Sox2*^{CreERT2} mice were crossed with *Gt(ROSA)26Sor*^{tdTom} reporter mice, and then crossed with *Atoh1*^{GFP} mice to generate the lineage tracing line. Notch gain-of-function mice were generated by breeding *Sox2*^{CreERT2}/ *Gt(ROSA)26Sor*^{tdTom} with *R26R*$^{stop\text{-}NICD\text{-}nGFP}$ (JAX, stock #008159, borrowed from Shahragim TAJBAKHSH lab)[22]. Presenilin1 deficient (*Psn*$^{-/-}$) mice (borrowed from Bart De Strooper) crossed with *Atoh1*^{GFP} mice to get *Atoh1*^{GFP}/*Psn*$^{-/-}$ mice. And Notch conditional knock out mice was generated by crossing *Notch1*^{flox} (purchased from JAX, stock #007181) with *Sox2*^{CreERT2}/ *Atoh1*^{GFP} mice. Mice were genotyped genomic DNA isolated from toe tissue. The primers used for genotyping were shown in table1.

Table 1. Primers for mouse genotyping

Gene Name	Forward	Reverse
Cre	CCAATTTACTGACCGTACACCAA	CTGATCCTGGCAATTTCGGCTA
tdTom	WT-AAGGGAGCTGCAGTGGAGTA Mut-CTGTTCCTGTACGGCATGG	WT-CCGAAAATCTGTGGGAAGTC Mut-GGCATTAAAGCAGCGTATCC
Atoh1^{GFP}	WT-GCGATGATGGCACAGAAGG	WT-GAAGGGCATTTGGTTGTCTCAG Mut-AGGGTCAGCTTGCCGTAGGT
Psn1	WT-GTAGGGGATATGATTTTCTTTTTG Mut-CATATACTGAAATCACAGCCAAG	WT-CCATTCGGGGAGGTACTTGATAA Mut-CGGATCAAGCGTATGCAGCCG
Notch^{flox}	TGC CCT TTC CTT AAA AGT GG	GCC TAC TCC GAC ACC CAA TA
NICD-nGFP	WT-AAG GGA GCT GCA GTG GAG TA Mut-TGG TAT GCC TGA CAC TCA CC	WT-CAG GAC AAC GCC CAC ACA Mut-ACA CCG GCC TTA TTC CAA

Tamoxifen Administration

Tamoxifen (TM, Sigma) or 4-Hydroxytamoxifen (4-OH, Sigma) was dissolved to a final concentration of 1mg/ml or 3mg/ml in 90% corn oil (Sigma) with 10% ethonal (Sigma). For *Sox2*^{CreERT2}/ *Gt(ROSA)26Sor*^{tdTom} / *Atoh1*^{GFP} mice, if collected the samples at embryonic stages, 0.1mg TM was intraperitoneal (i.p.) injected into per pregnant female at E9.5 or E10.5. If collected the samples at postnatal stages, each pregnant female was injected 0.03mg TM (i.p.) at E10.5. For *Sox2*^{CreERT2}/*Gt(ROSA)26Sor*^{tdTom}/*R26R*$^{stop\text{-}NICD\text{-}nGFP}$ mice and *Sox2*^{CreERT2}/ *Notch1*^{flox} mice, 0.1ml 4-OH TM or TM (3mg/ml) was injected into the pregnant females (i.p.) at E8.5, respectively.

RNA extraction and Real time PCR (RT-PCR)

Total RNA was isolated from whole cerebellar tissue samples at E13 using Trizol Reagent (Invitrogen). The RNA concentration was measured by a spectrophotometer (NanDrop1000; Thermo) followed by a reverse transcription process using PrimeScript RT reagent kit (Roche). Real time PCR analysis was performed using SYBR green mix (Roche) and the values were normalized to β-actin values. The primer pairs for different genes are as follows: Atoh1, sense 5'-CCCAATGTCGGAGAGCAACC-3' and anti-sense 5'-TCCTCGAAGGCTGGGAAGTG-3'; Ptf1a, sense 5'-TAGACACGCTGC GGCTGCGCTTGGCCATAGGCTACA-3' and anti-sense 5'-ACAAAGACGCGG CCAACCCGATGTGAG-3'; Olig2, sense 5'-CGCAAGCTCTCCAAGATCG-3' and anti-sense 5'- CTCACCAGTCGCTTCATCTC-3'. β-actin, sense 5'- TCCATCATGAAGTGTGACGT-3' and anti-sense 5'-GAGCAATGATCTTGATCTTCAT -3'. PCR conditions used here were denaturing at 95 °C for 10 s, followed by 40 cycles of 95 °C for 5 s and 60 °C for 30 s. Data were analyzed using the comparative threshold cycle (Ct) method, and results were expressed as fold difference normalized to β-actin.

Immunohistochemistry and antibodies

For the samples collection, embryos before E13.5 were fixed in 2% paraformaldehyde (PFA) in PBS at 4 °C for 2-3 hours, and embryos after E13.5 but before born first were perfused with

2% PFA, then post-fixed for 24 hours. Whereas, samples which were collected at postnatal stages, perfused the mice with 1 X PBS, followed by 4% PFA perfusion, and then post-fixed in 4% PFA for another 24 hours. Dehydrated embryos or the whole head in 30% sucrose in 1 X PBS overnight (o/n). After all the samples sank into the bottom of the tube, embedded them in OCT compound (TissueTek) and frozen at -20 °C. Sagittal sections were made by cryostat (Leica) at 20 μm and then stored slices at -80 °C. For the immunostaining, sections were fixed with 4% PFA for 10 minutes at room temperature (RT), then blocked with 10% normal donkey or goat serum in 1 X PBS with 0.1% Triton (PBT) for 1 hour at RT followed by 3 times washing in 1 XPBT. Thereafter, these sections were incubated with primary antibodies diluted in 0.1% 1 X PBT containing 1% normal donkey or goat serum o/n at 4 °C or 3-4 hours at RT. After 3 times washing with 1 X PBT, incubated with appropriate secondary antibodies conjugated with Alexa Fluor 488, Alexa Fluor 555, or Alexa Fluor 647 (1:500, Invitrogen) in 0.1% 1 X PBT containing 1% normal donkey or goat serum for 1-2 hours at RT. Washed with 1 X PBT for 3 times, then counterstained the slides with DAPI (1:2000, Sigma) and mounted by using Vectashield (Vector) after rinsing. Antigen retrieval was performed by using 10 mM sodium citrate buffer, pH 6.0, boiled 5 minutes in microwave, and cooled down in RT for about 20 minutes for Lhx1/5 and Olig2 staining. Primary antibodies used in this study were rabbit anti-Sox2 (1:500, Millipore, AB5603), rabbit anti-Ptf1a and Rabbit anti-Atoh1 (1:200, a kind gift from Dr. Mikio Hoshino, National Center of Neurology and Psychiatry · Department of Biochemistry and Cellular Biology, Japan), rabbit anti-Calbindin (1:500, Immunostar, 24427), rabbit anti-Pax6 (1:300, Biolegend: PRB-278P), rabbit anti-Pax2 (1:200, Thermo, QE215176), mouse anti-Lhx1/5 (1:100, DSHB, AB_531784), goat anti-Olig2 (1:500, R&D systems, AF2418) and Guinea pig anti-Tbr1 (1:500, Synaptic Systems, 328 005). After staining, images were obtained by using confocal microscope (Olympus FV-1200 or Leica SP8).

Cell counts

Confocal images for single layer scanning of sagittal cerebellar sections were calculated for each developmental stages (E11.5, E12 and E13) after DAPI staining. Each section took the average of the four values that obtained from 4 single layer calculating, which could form a Z stack. And each cerebellar samples counted 6-8 sections that took from the beginning to the end of the cerebellum. All quantifications were done blinded to the genotyping. For each stage littermates were analyzed and all groups of quantifications were carried out from at least 3 individuals.

scRNAseq quantification and statistical analyses

Aligned 10X data were retrieved from ENA: PRJEB23051 data set for the following samples: E10, E11, E12 and E13. Umitools has been used to generate gene-cell matrices with the following parameters: --extract-umi-method=tag, --umi-tag UB, --cell-tag CB, --per-gene, --gene-tag GX, --per-cell. Genes not expressed in any cells were removed from considerations, as were all mitochondrial and ribosomal protein genes. To remove likely dead or multiplet cells from downstream analyses, cells were discarded if they had less than 3500 UMIs, greater than 15000 UMIs, or were composed of over 10% mitochondrial UMIs. The final dataset was composed of 14637 cells and 18937 genes. Then Seurat bioconductor package v2.3.4[23] has been used to do cell-cell comparison and identify cell types. First, we performed a t-SNE (t-distributed stochastic neighbor embedding) with the first 20 principal components after application of PCA reduction. This allowed us to visualize the grouping of cells and the expression of genes of interest. Expression of cells in 3 populations has been represented with boxplot and differential expression between the 3 populations has been calculated with a Welch two sample t-test procedure.

Monocle 2.6.4[24] was used to infer the pseudotime trajectory. As we worked with UMI count data, we assumed that the data were distribued among a negative binomial distribution with fixed variance. The genes that "define progress" were selected using the unserpervised procedure "dpFeature": we first selected genes expressed in at least 5% of all the cells. We then run reduceDimension with tSNE as the reduction method, num_dim=10", norm_method="log" and max_components = 2. Finally cells were clustered with the density peak clustering algorithm by setting P to 2 and Δ to 5 (and skip_rho_sigma = T to facilitate the computation). The top 1000 significantly differentially expressed genes between clusters were selected as the ordering genes. The state 3 where Sox2 is expressed and Atoh1 not expressed was defined as the start of the pseudotime. The seurat FindMarkers function was used to identify the top 10 genetic markers of each lineage state's.

MADM Mouse Lines and Maintenance

MADM employs Cre recombinase/loxP-dependent interchromosomal recombination highlighting two scenarios: (i) Recombination occurs in G2 phase of the cell cycle will exhibit X segregation (G2-X MADM clone) which can create two distinctly labelled daughter cell lineages from their common mother progenitor cell; (ii) Recombination occurs in G1 phase or in G2 phase followed by Z segregation (G1/G2-Z MADM clone), one or both daughter cell lineages will be labelled in yellow. Mouse protocols were reviewed by institutional ethics committee and preclinical core facility (PCF) at IST Austria and all breeding and experimentation was performed under a license approved by the Austrian Federal Ministry of Science and Research in accordance with the Austrian and EU animal laws. Mice were maintained and housed in animal facilities with a 12-hour day/night cycle and adequate food/water conditions according to IST Austria institutional regulations. Mouse lines with Chr. 11 MADM cassettes (MADM-11^{TG} JAX stock #013751, and MADM-11^{GT} JAX stock #013749), and *Sox2-CreER* (JAX stock #017593) have been described previously [25,26]. All MADM-based analyses were carried out in a mixed C57BL/6J, CD1 genetic background.

Generation of MADM Clones in Cerebellum and Tissue Collection

To induce MADM labeling, *MADM-11*$^{GT/GT}$*/Sox2*^{CreER} were crossed with *MADM-11*$^{TG/TG}$ in order to generate experimental mice *MADM-11*$^{GT/TG}$*/Sox2*^{CreER}. The day of observed vaginal plug was defined as E0 to monitor gestation days. Pregnant mice were injected i.p. with TM (2-3 mg/pregnant female) (Sigma) dissolved in corn oil (Sigma) at E11 to induce MADM clones. Live embryos were recovered at E18–E19 through cesarean section, fostered, and raised until further analysis. At P21 experimental MADM mice were deeply anesthetized through injection of a ketamine/xylazine/acepromazine solution (65 mg, 13 mg and 2 mg/kg body weight, respectively), and confirmed to be unresponsive through pinching the paw. Mice were perfused transcardially with 4% PFA in phosphate-buffered saline (PBS, pH 7.4). Brains were removed and postfixed o/n at 4°C to ensure complete fixation. Brains were washed with PBS, and cryopreserved with 30% sucrose solution in PBS for approximately 48 hr. Brains were then embedded in Tissue-Tek O.C.T. (Sakura). For the analysis of MADM labeling, 30-45μm sagittal sections were directly and consecutively collected and fixed to superfrost glass slides (Thermo Fisher Scientific). Sections were washed 3 times for 5 min with PBS, followed by staining with the nuclear stain DAPI (Invitrogen). After this step the slides were again washed 3 times with PBS and embedded in mounting medium containing 1,4-diazabicyclooctane (DABCO; Roth) and Mowiol 4-88 (Roth).

Imaging and analysis of MADM-labeled brains

Sections were imaged using an inverted LSM800 confocal microscope (Zeiss) and processed using Zeiss Zen Blue software. Confocal images were analyzed in Photoshop software (Adobe) by manually counting MADM-labeled cells. Cerebellar areas were identified by using the Allen Brain Atlas (http://mouse.brain-map.org/static/atlas).

Cerebellar Organoids labeling and staining

Human iPS cells (iPSCs, ATCC-DYS0100) were maintained in self renewal on a layer of geltrex (Gibco, A14133-01), in E8 Basal Medium (Gibco, A15169-01) supplemented with E8 Supplement (50X). iPSC were dissociated with EDTA (Invitrogen) 0.5mM, pH 8.0, for 3 minutes incubation, to maintain cell clusters. Cerebellar organoids were culture as described by Muguruma et al and Ishida et al. [10,27], and were electroporated at 25 days of differentiation protocol with 33,3 ug of pGL3_Sox2_Cre and 66,6 ug of pCAG_LSL_Venus_NLS (the 24h experiment) or with 20 ug of pGL3_Sox2_Cre, 20 ug pPBase, 80 ug pCAG_LSL_Venus_NLS (the 16d experiment). Organoids were transferred inside the Electroporation cuvettes (VWR, ECN 732-1136, 2mm) resuspended in Buffer 5 (under patent) and electroporation was performed with the Gene Pulser XcellTM. Organoids were fixed at 26d or 41d of differentiation with 4% PFA, cryoprotected in 20% sucrose and embedded in Frozen Section Compound (Leica, 3801480). Organoids were cryosectioned at 40 µm with Leica CM 1850 UV Cryostat. Immunofluorescence staining were performed on glass slides. Blocking and antibody solutions consisted of PBS supplemented with 3% goat serum, 0.3% Triton X-100 (Sigma). Primary antibodies were incubated overnight at 4°C and secondary antibodies for 1 hour at RT. Primary antibodies used were Chicken anti-GFP (1:2000, abcam, ab13970), Rabbit anti-Sox2 (1:500, abcam, ab97959), Mouse anti-Pax6 (1:100, SantaCruz, sc-53108)and Rabbit anti-Calbindin (1:500, Sigma, c2724-2). Nuclei were stained with 1 µg/ml DAPI (Sigma). Sections and coverslips were mounted with Permanent Mounting Medium.

Statistical analysis

Statistical analyses were performed using GraphPad Prism software (GraphPad Software Inc., La Jolla, CA, USA). N values refers to independent animals and are detailed in the figure legends. All data are presented as mean ± SEM. Statistical testing was based on t-tests or one-way ANOVA, followed by Tukey's honest significant test.